Journal of Electrochemistry

Volume 28 | Issue 1

2022-01-28

A High-Performance Continuous-Flow MEA Reactor for Electroreduction CO_2 to Formate

Pei-Xuan Liu

Lu-Wei Peng

Rui-Nan He

Lu-Lu Li

Jin-Li Qiao
1. College of Environmental Science and Engineering, Donghua University, Shanghai 201620, China;2. Shanghai Institute of Pollution Control and Ecological Security, Shanghai 200092, China;,
qiaojl@dhu.edu.cn

电 化 学
J. Electrochem. 2022, 28(1), 2104231 (1 of 9)

【Article】 **DOI**: 10.13208/j.electrochem.210423 **Http**://electrochem.xmu.edu.cn

A High-Performance Continuous-Flow MEA Reactor for Electroreduction CO_2 to Formate

Pei-Xuan Liu[1#], Lu-Wei Peng[1#], Rui-Nan He[1], Lu-Lu Li[1], Jin-Li Qiao[1,2*]

(*1. College of Environmental Science and Engineering, Donghua University, Shanghai 201620, China;*
2. Shanghai Institute of Pollution Control and Ecological Security, Shanghai 200092, China)

Abstract: The electrochemical carbon dioxide reduction reaction (CO_2RR) is a promising approach to produce liquid fuels and industrial chemicals by utilizing intermittent renewable electricity for mitigating environmental problems. However, the traditional H-type reactor seriously limits the electrochemical performance of CO_2RR due to the low CO_2 solubility in electrolyte, and high ohmic resistance caused by the large distance between two electrodes, which is unbeneficial for industrial application. Herein, we demonstrated a high-performance continuous flow membranes electrode assembly (MEA) reactor based on a self-growing Cu/Sn bimetallic electrocatalyst in 0.5 mol·L^{-1} $KHCO_3$ for converting CO_2 to formate. Compared with an H-type cell, the MEA reactor not only shows the excellent current density (66.41 mA·cm^{-2} at -1.11 V_{RHE}), but also maintains high Faraday efficiency of formate (89.56%) with the steady work around 20 h. Notably, we also designed the new CO_2RR system to effectively separate the gaseous/liquid production. Surprisingly, the production rate of formate reached 163 μmol·h^{-1}·cm^{-2} at -0.91 V_{RHE} with the cell voltage of 3.17 V. This study provides a promising path to overcome mass transport limitations of the electrochemical CO_2RR and to separate liquid from gas products.

Key words: electrochemical reduction; carbon dioxide; flow MEA reactor; electrolyzer

1 Introduction

The excessive consumption of fossil fuel by anthropological behavior has caused the increasing CO_2 concentration level in the atmosphere, thus, intriguing serious concerns for environmental problems and energy crisis[1, 2]. To solve the above problems, there are several protocols for delimiting CO_2 emission into air, such as chemical conversion, photocatalytic reduction, thermo-catalytic and electrochemical CO_2 methods[3-5]. Among all these protocols, electrochemical CO_2 reduction reaction (CO_2RR) is the most attractive strategy to convert CO_2 into fuels and valuable chemicals via renewable energy sources (wind, solar and hydro) in mild pressure and normal atmospheric temperature[6]. The products of CO_2RR include C_1 products (CO, formate, CH_3OH) and C_{2+} products (C_2H_4, CH_3CH_2OH), while formate or formic acid, due to its high hydrogen content and easy handling (transport and storage) at room temperature, can be usually applied in fuel cells[7]. Furthermore, formate is also treated as a key intermediate and starting material for the chemical synthesis industry such as electrowinning, leather tanning, and aircraft de-icing[8, 9]. Unfortunately, most researchers in CO_2RR just put their efforts on the development of electrocatalysts tested in the H-type reactor so far[10-14], because the standard H-type reactor is broadly used to initially evaluate the intrinsic activity and selectivity of CO_2RR electrocata-

Cite as: Liu P X, Peng L W, He R N, Li L L, Qiao J L. A high-performance continuous-flow MEA reactor for electroreduction CO_2 to formate. *J. Electrochem.*, 2022, 28(1): 2104231.

Received: 2021-04-23, Revised: 2021-06-06. #Same contribution to this work. *Corresponding author, Tel: (86-21)67792379, E-mail: qiaojl@dhu.edu.cn

lysts due to its simple fabrication[15]. However, the H-type reactor has certain limitations, such as large electrode distance, low CO_2 solubility in the electrolyte and large pH gradient close to the surface of the electrode, which definitely causes the limitation of CO_2 mass transfer in the aqueous and the inferior performance of CO_2RR.

In order to meet the demands of industrial application for CO_2RR, developing the reaction system is an urgent job to achieve sufficient rate of CO_2 conversion and high current density[16]. As the core part of reactionsystem, the electrolyzer includes H-type flow-cell, 3-compartment cell configuration and membrane electrode assembly (MEA) reactor. An H-type flow-cell is based on the traditional H-type reactor, while the anolyte and catholyte are continuously circulated by peristaltic pumps. CO_2 dissolved in the continuous catholyte can be transported to the interface of gas-liquid-catalyst, where CO_2 is reduced to various products, namely formic acid, methanol, CO, ethylene, etc. This H-type flow-cell can enhance gas-liquid mass transfer of CO_2 by circulating catholyte, however, the products of CO_2RR might cross over the separated membrane from cathode to anode[17]. Noticing this problem, Yang et al.[18] designed a 3-compartment cell configuration to produce formic acid directly. The 3-compaertment cell configuration consisted of a cathode compartment, an anode compartment and a center flow compartment. In this system, there can be an anion-exchange membrane between a cathode compartment and a center flow compartment, and a cation-exchange membrane between an anode compartment and a center flow compartment, which can perfectly collect anodic and cathodic products of CO_2RR. As yet, the addition of center flow compartment would definitely increase the distance between cathode and anode, thus, causing highly inherent cell resistance. In order to effectively reduce the internal resistance and ohmic polarization, MEA with near zero distance between a cathode and an anode has attracted lots of attention[19, 20]. In the MEA reactor, the electrocatalysts are always loaded on hydrophobic carbon paper as a gas diffusion electrode (GDE), which can allow CO_2 molecules to be directly reduced to various products. Nevertheless, the channel of CO_2 transport would be prohibited by the flooding of the gas diffusion layer and the evaporation of the catholyte, therefore, water management is essential to keep a stable gas-liquid of GDE[21, 22]. Thus, it is necessary to design a new type of reaction devices to enable the widely used of CO_2RR for practical applications.

Considering all the challenges of an H-type flow-cell, a 3-compaertment cell configuration and a membrane electrode assembly (MEA) reactor, in this work, we designed a novel MEA-based flow cell by the combination of H-type flow-cell and MEA reactor. From one side, the circulation of catholyte can facilitate the diffusion of CO_2 to the surface of electrcatalysts. From the other point, MEA reactor can largely shorten the internal resistance and reduce ohmic polarization between cathode and anode. As a result, the as-designed flow MEA reactor showed excellent formate selectivity (89.56%), high current density (47.56 $mA \cdot cm^{-2}$ at -0.91 V_{RHE}) and durable stability (20 h), which is superior to the H-type reactor owing to the higher solubility of CO_2, shorter distance between the electrodes, lower ohmic resistance and charge transfer resistance of flow MEA reactor. As such, we also explore the influence of different electrolytic environments in the flow MEA reactor, such as bubbling CO_2 gas in electrolyzer and different usages of anion-exchange membrane (AEM) or cation-exchange membrane (CEM). Based on the above points, we demonstrated that this novel home-made flow MEA reactor can realize current density almost 3 times greater than the H-type reactor at -0.91 V_{RHE} with the relatively low cell voltage at 3.17 V.

2 Experimental

2.1 Materials

Potassium hydroxide (KOH), potassium bicarbonate ($KHCO_3$), tin(II) chloride dihydrate ($SnCl_2 \cdot 2H_2O$), copper(II) chloride dihydrate ($CuCl_2 \cdot 2H_2O$), trisodium citrate dehydrate ($Na_3C_6H_5O_7 \cdot 2H_2O$) and urea ($CH_4N_2O$) were purchased from Sinopharm Chemical

Reagent Co. Ltd. Carbon cloth (WOS 1009) was purchased from Phychemi (HK) Limited Company. All the chemicals were analytical grade and used in experiments without further purification.

2.2 Preparation of the Electrodes

Nitrogen doped carbon cloth (N-CC) was prepared via the method reported in our previous work[23]. Specifically, 2.941 g $Na_3C_6H_5O_7 \cdot 2H_2O$ (0.01 mol) and 0.6 g CH_4N_2O (0.01 mol) were mixed with 0.39 g $SnCl_2 \cdot 2H_2O$ (0.01 mol) and 0.0684 g $CuCl_2 \cdot 2H_2O$ (0.01 mol) in 100 mL deionized water stirring for complete dissolution. Then, 0.68 g $CHNaO_2$ (10 μmol) was added in the mentioned clear solution, which was stirred to a transparent solution and sonicated for 30 min. The bimetallic Cu/Sn was co-electrodeposited onto the porous N-CC at the constant voltage (-0.75 V_{SCE}) for 6 h in a three-electrode configuration, where a piece of 0.8 mm graphite rod was used as the anode, the N-CC (20 mm ~ 10 mm) was severed as the cathode and a saturated calomel electrode (SCE) was applied as the reference electrode.

2.3 Experimental Set Up

The continuous flow experiments were performed in a flow-cell system in Figure 1, and the comparative experiments were performed in the traditional H-type reactor with a three-electrode system (Figure S1), where the as-prepared bimetallic Cu/Sn was used as the working electrode, Ag/AgCl as the reference electrode and Pt film as the counter electrode. The flow-cell system in Figure 1(A) consisted of a flow MEA reactor, several Teflon plates, two peristaltic pumps, a gas-liquid separation device for cathode and electrolyte circulation device for anode, while the core MEA reactor with a sandwich structure was made of Cu/Sn electrode, an anion-exchange membrane (FAD, Germen) or a cation-exchange mem-brane (Nafion 117, DuPont) and Pt film. The effective Cu/Sn electrode area is 2 cm^{-2} and the distance between working electrode and counter electrode is 4 mm. It was worth noting that, CO_2 gas can bubble inside the MEA reactor. In addition, CO_2 gas was also continuously purged into the $KHCO_3$ solution (150 mL) at least 30 min, and then the CO_2-saturated 0.5 mol·L^{-1} $KHCO_3$ solution was circulated into MEA reactor by using a peristaltic pump (HUXI, HL-25), and the flow rate of the electrolyte was 13 mL·min^{-1}. After CO_2 was electrochemically reduced in the MEA reactor, the liquid product and gas product following the $KHCO_3$ solution were circulated back to the gas-liquid separation device to achieve an automatic separation. In the anode part, 0.5 mol·L^{-1} KOH solution (100 mL) was circulated by another peristaltic pump and oxygen evolution reaction was produced by the oxidization of OH^-. The electrolysis was carried out with the liquid phase environment in both cathode and anode.

2.4 Electrochemical Test and Physicochemical Characterization

All the electrochemical measurements were performed by CHI660E electrochemical workstation

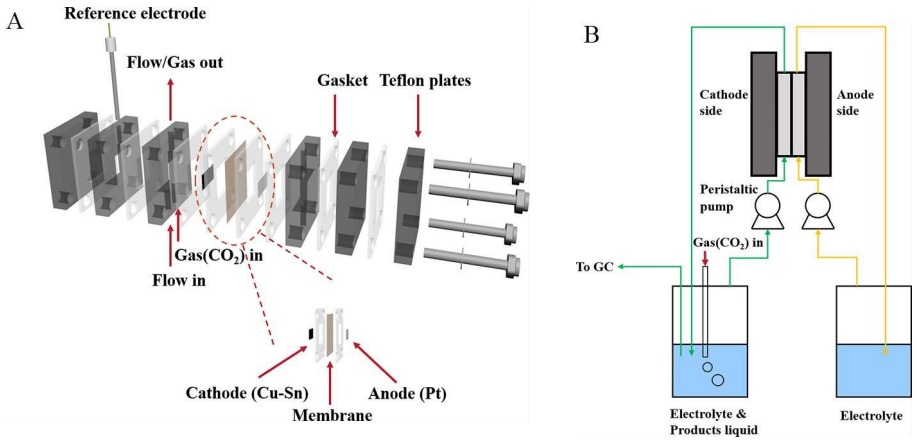

Figure 1 Schematic of the flow MEA reactor (color on line)

(Shanghai Chenhua). Before the electrochemical test of CO_2 reduction, the cathode electrolyte solution was saturated with highly-pure nitrogen (99.999%) in order to expel oxygen from the solution. Cyclic voltammetry (CV) and linear sweep voltammetry (LSV) were employed to confirm the difference of current density in N_2 and CO_2 saturated condition upon different applied potentials. The scan rates of CV and LSV were 50 and 5 $mV \cdot s^{-1}$ at room temperature in a three-electrode system. Electrochemical impedance spectroscopic (EIS) test was conducted at -0.91 V_{RHE} with the amplitude of 0.1 V over the frequency range from 0.1 to 100 kHz. One-hour potentiostatic experiment and 20-hour stability test were conducted by using the amperometric mode (*i*-*t* curve).

In electrochemical CO_2 reduction reaction, the cathode electrolyte was CO_2-saturated $KHCO_3$ (0.5 $mol \cdot L^{-1}$) at a pH of 7.5. Without further explanation, the potential described below will be versus reversible hydrogen electrode (RHE) that can be converted against SCE by using the following equation.

$$E(\text{vs. RHE}) = E(\text{vs. SCE}) + 0.1972 + 0.0591\text{pH} \quad (1)$$

The scanning electron microscope (SEM) was used to analyze the surface morphology by a S-4800 field-emission at 5 kV. The X-ray diffraction (XRD) analysis was carried on a Philips PW3830 X-ray diffractometer by using a Cu K_α radiation at 40 mA and 40 kV. Before the XRD test, all the samples were kept in a little bottle filled with nitrogen, in order to avoid oxidation. Liquid products were quantified by an Ion Chromatography instrument (IC1820, Shanghai Sunny Hengping Scientific instrument Co. Ltd). Before the liquid products were injected into the ion chromatography, the liquid samples were diluted 10 or 20 times with purified water. The Faradaic efficiency for formate was calculated according to the following equation.

$$FE_{HCOO^-}(\%) = \frac{2 \times n \times F}{Q} \times 100\% \quad (2)$$

Where, 2 is the number of electrons transferred from one CO_2 molecule to one $HCOO^-$; n is the molar concentration of the $HCOO^-$; F is the Faraday constant (96485 $C \cdot moL^{-1}$); Q is the total charge during the working electrode.

Gaseous products were collected by the online gas chromatography system (GC-2014C, Shimadzu), assembled with TCD-2014C and FID-2014C. Before the CO_2 carrying gas products were injected into the gas chromatography system, the gas samples were dehumidified by a filter bundle kit. The Faradaic efficiency for gas products (CO and H_2) can be calculated according to the following equation.

$$FE_{gas}\text{-}(\%) = \frac{\frac{v}{60\ s \cdot min^{-1}} \times \frac{c}{24000\ cm^3 \cdot mol^{-1}} \times n \times F}{J_{total}} \times 100\% \quad (3)$$

Where, v is the CO_2 flow rate, n is the number of electrons transferred from one CO_2 molecule to H_2/CO, c is the molar concentration of the gaseous product.

3 Results and Discussion

3.1 Characterization and Formation Mechanisms of Electrode

The SEM images were used to analyze the microstructure and morphology of the electrode during the twenty-hour electrolysis experiment, as shown in Figure 2(A-E). The bimetallic Cu/Sn electrode with a 3D-multilayered microstructure showed some cavities on the surface (Figure 2(A)), which could provide a large electrochemical surface area and confine the intermediates of reduced CO_2 in order to generate $HCOO^-$. It can be observed that this 3D-multilayered microstructure was almost unchanged in the first 10 h (Figure 2(C)). After 20-h electrolysis, it can be found that the cavities on the surface of electrode were partly filled and some thorns also appeared along the edge of Cu/Sn electrode (Figure 2(E)). These might be caused by the slightly changed morphology of bimetallic electrode according to the flushing of the flowing electrolyte.

The XRD patterns of the Cu/Sn electrode were measured to analyze crystal phases during 20-h stability test in Figure 2(F), which shows the small peaks at 32.108 °, 44.902 °, 55.33 °, 64.576 ° and 79.47 ° ascribing to the (101), (211), (301), (321), (312) planes

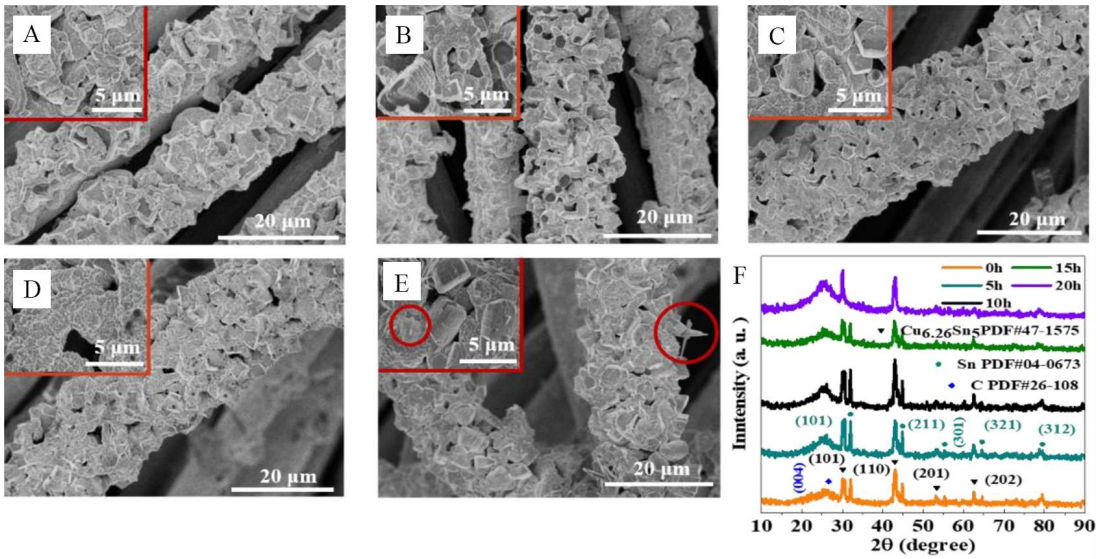

Figure 2 SEM images: (A) before and after different electrolysis time. (B) 5 h, (C) 10 h, (D) 15 h and (E) 20 h. (F) XRD patterns obtained before and after different time. (color on line)

of Sn (JCPDS card no. 04-0673), respectively. To our surprise, the diffraction patterns of Cu/Sn electrode after 15-h electrolysis showed no changes. However, the two diffraction peaks at 30.126° and 42.971° became predominant after 20-h electrolysis, well indexed to the (101) and (110) planes of alloy $Cu_{6.26}Sn_5$ (JCPDS card no. 47-1575), which could affirm that the (101) and (110) planes of alloy $Cu_{6.26}Sn_5$ are the main active crystal planes for CO_2RR. The disappearance of the Sn peak may be caused by the loss of Sn particles from the electrode surface. Interestingly, the intensity of carbon peaks (004) (JCPDS card No. 26-108) revealed an increasing trend along with the increased electrolysis time, which may prove that the Cu/Sn atoms were peeled off due to flushing of the flowing electrolyte.

3.2 Electrochemical Analysis

Considering the degradation of the IrO_2 on carbon paper in the anode by a drop-cast method[24], Pt was utilized as an anode electrode for oxygen evolution reaction. For CV and LSV tests, the electrolyte solution (0.5 mol·L^{-1} $KHCO_3$) was saturated with highly-pure nitrogen in order to expel oxygen absorbed in the electrolyte and then continuously purged with highly-pure CO_2. CV and LSV data were collected at a potential window between -0.61 and -1.11 V_{RHE} through the N_2 and CO_2-saturation $KHCO_3$. From Figure S2, the current densities at different applied potentials in CO_2-saturated electrolyte was obviously much larger than those in N_2-saturated condition. Considering that the working electrode and the counter electrode are in close contact, the distance between an anode and a cathode is greatly shortened, thus, reducing the ohmic resistance between the two electrodes. Besides, the circulation of electrolyte by peristaltic pumps is favorable for mass transfer of CO_2 to the surface of Cu/Sn electrode and promotion of CO_2 solubility in 0.5 mol·L^{-1} $KHCO_3$ by directly bubbling CO_2 into MEA assembly.

Figure 3(A) provides the LSV curves of different MEA assemblies and H-type reactor. Compared with the H-type reactor, the current density of the flow MEA reactor by bubbling CO_2 inside was 66.41 mA·cm^{-2} at -1.11 V_{RHE}, which is two times higher than that of the H-type reactor (30.05 mA·cm^{-2}). The onset potential for CO_2RR is used to evaluate the overpotential of catalytic electrode, which can indirectly evaluate the activity of the cell efficiency[20]. It is worth noting that the onset potential of the Cu/Sn electrode was -0.57 V_{RHE} at 2 mA·cm^{-2} in the flow MEA reactor with CO_2 purging inside, which had a positive shift of more than 80 mV compared with -0.65 V_{RHE} of the H-type

cell. In addition, the Cu/Sn electrode in MEA reactor without bubbling CO_2 showed the onset potential of -0.64 V_{RHE} (similar to the H-type reactor), implying that bubbling CO_2 into MEA assembly can reduce the gas diffusion resistance. Overall, the flow MEA reactor with CO_2 bubbling inside can acquire higher cell efficiency and current density than the H-type cell.

In order to further investigate the working principle of the flow MEA reactor, the Nyquist plots at -0.91 V_{RHE} are shown in Figure 3(B). The ohmic resistance is the value of abscissa according to the starting point of EIS curve. From Figure 3(B), the ohmic resistance of the flow MEA reactor was merely 0.957 Ω, near three times lower than that of the H-type reactor (3.05 Ω), implying that the former has better CO_2RR performance than the latter due to the reduced electrode distance. Moreover, the charge transfer resistance (CTR) is related to the radius of semicircle in EIS curve. The CTR of the flow MEA reactor was 0.996 Ω, much smaller than that of the H-type reactor (4.85 Ω), demonstrating that the flowing electrolyte does increase the diffusion rate of electrons. Actually, the CTR has a close relation with current density, which can be observed in Figure S3. The reactor system with a lower CTR showed a higher total current density, manifesting a higher CO_2 consumption rate. In addition, the current density of the flow MEA reactor with CO_2 purging inside was unstable, possibly due to the precipitation of carbonate in the system[16].

To gain insight into the influence of different applied potentials, the Faraday efficiency (at -0.91 V_{RHE}) and current density at different potentials are shown in Figure 3(C) and Figure S4. It can be observed that in the potential range from -0.61 to -1.11 V_{RHE}, the distribution of gaseous and liquid products displayed remarkable changes along with potentials. The FE_{HCOO^-} of Cu/Sn electrode in the flow MEA reactor with CO_2 purging inside had a dramatic increase from 36.51% to 72.82% in a potential range from -0.61 to -0.81 V_{RHE}, and reached the maximum selectivity of 89.56% at -0.91 V_{RHE}, then finally slightly decreased at -0.91 and -1.01 V_{RHE}. The decrease of FE_{HCOO^-} in the flow MEA reactor may be the limitation of mass transport of CO_2 intermediate at high overpotentials due to the rapid consumption of CO_2[25]. Under the same conditions, the FE_{HCOO^-} of the H-type reactor in Figure S5 firstly showed a similar tendency as the flow MEA reactor between -0.61 and -0.81 V_{RHE}, then, maintained more than 90% after reaching the maximum level of 90.24% at -1.01 V_{RHE}. Furthermore, the FE_{HCOO^-} of Cu/Sn electrode in the flow MEA reactor without bubbling CO_2 inside was 81.49% at -0.91 V_{RHE}, lower than that with bubbling CO_2 into electrolyser (Figure 3(D) and Figure S6), demonstrating further that bubbling CO_2 into MEA assembly can promote FE_{HCOO^-} by accelerating the diffusion of CO_2 toward the surface of Cu/Sn electrode. For gaseous products, there were only CO and H_2 detected by the online gas chromatography in the flow MEA reactor. In contrast, the lower HER of the flow MEA reactor than the H-type cell may be due to the higher local pH close to the surface of Cu/Sn electrode, and thus, hydrogen binding energies would be weakened in the flow MEA reactor[26]. The energy efficiency (EE) approached 31%.

In order to meet the industrial demand for CO_2RR, the stability of the flow MEA reactor was evaluated at -0.91 V_{RHE} in Figure 3(E). During the first 12 h, the flow MEA reactor showed a relatively stable FE_{HCOO^-} of ~89%. The current density and FE_{HCOO^-} became a slight oscillation due to the rapid consumption of CO_2 and the excessive accumulation of formate close to the surface of the Cu/Sn electrode. FE_{HCOO^-} was 80% at the current density near 50 $mA \cdot cm^{-2}$ in the last 8 h. This degradation of FE_{HCOO^-} and the increase of current density can be partially attributed to changes in surface morphology of Cu/Sn electrode in the last 8 h as shown in SEM images, suggesting that the CO_2RR performance is directly related to the microstructure of Cu/Sn electrode. As observed in Figure 2(F), the XRD patterns displayed the strong diffraction peaks at 30.126° and 42.971° in the last 10 h, demonstrating that the active $Cu_{6.26}Sn_5$ (110) and (101) crystal planes can be effectively worked even in the

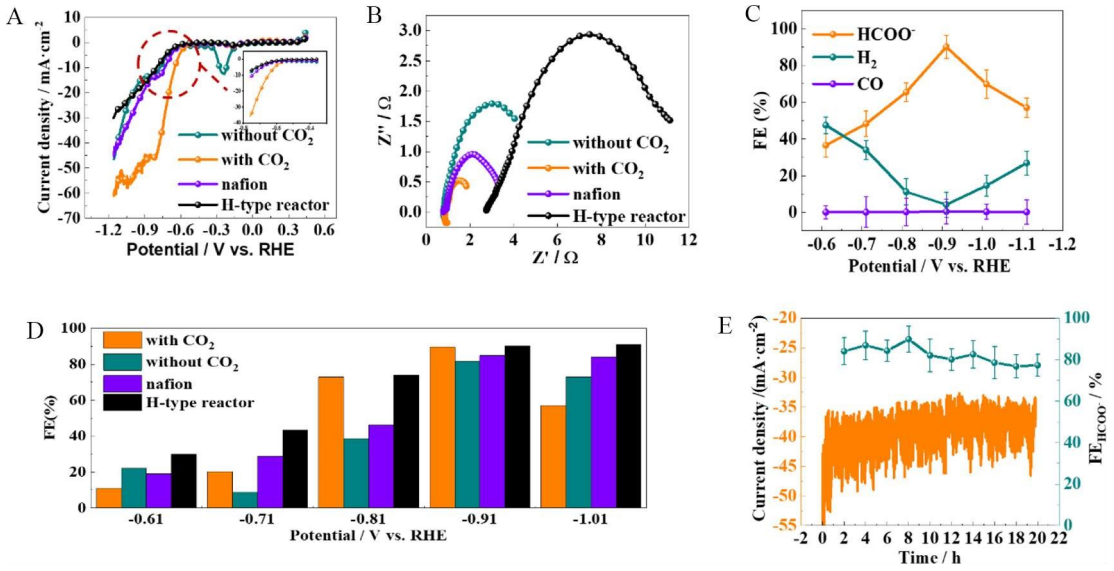

Figure 3 (A) LSV results of the different MEA assemblies (with/without bubbling CO_2 inside; using Nafion/anion-exchange FAD membrane) and H-type reactor. (B) EIS curves for the different MEA assemblies in 0.5 mol·L^{-1} $KHCO_3$ solution at -0.91 V_{RHE} with a frequency range 0.5 ~ 100000 Hz. (C) FE at -0.91 V_{RHE}. (D) FE of formate for different MEA assemblies (E) Stability performance of the flow MEA reactor at the constant potential of -0.91 V_{RHE}. (color on line)

continuously 20-h electrolysis. The total production rate of formate during 20-h electrolysis had a slight decrease from ~177 μmol·cm^{-2} at the initial stage to ~163 μmol·cm^{-2} after 20-h electrolysis, but still ~2 times higher than those in the case for the H-type reactor (51.14 μmol) and without bubbling inside (69.64 μmol). In addition, the stability of CO_2RR performance also can be verified by LSV curves whichwere collected after each one-hour potentiostatic experiment in Figure S7. Not surprisingly, all the LSV curves coincided with each other, which can further prove the good stability of Cu/Sn electrode in the flow MEA reactor. The home-made flow MEA reactor performed excellent formate selectivity (89.56%), great current density (66.41 mA·cm^{-2}) at -1.11 V_{RHE} and durable stability (20 h), which is superior to those already reported in literature for CO_2RR (Table S1).

Besides, the polymer electrolyte membrane (PEM) was used to separate the anode and cathode for preventing the crossover of CO_2RR product. In order to explore the impact of different membranes on CO_2RR, the cation-exchange membrane (CEM) and anion-exchange membrane (AEM) were investigated in the flow MEA reactor. As shown in Figure 3(A), the current density of the Cu/Sn electrode by using the AME as a separator was 47.56 mA·cm^{-2} at -0.97 V_{RHE}, which is obviously higher than that by using the CEM (23.51 mA·cm^{-2}). Figure 3(C) and Figure S9 show the FE_{HCOO^-} values of the AEM and CEM, the former realized a FE_{HCOO^-} up to 89.56% at -0.96 V_{RHE}, which is higher than 84.87% of the later. Although the ion conductivities of the membranes are Nafion 117 > FAD, the current density and FE of formate by using the AME are better than using the CEM. The reasons can be from different functions of membranes. According to the equations of (1,3,4), the AEM can allow the OH^- running through a cathode to an anode. Thus, the production of OH^- by CO_2RR can be quickly transferred to an anode. As for a CEM, it will benefit the H^+ transferring from an anode to a cathode, and the evident hydrogen evolution will occurin a cathode by using a CEM as a separator. As can be seen in Figure S9, the FE of hydrogen by using the CEM as a separator was higher than that by using the AME.

CO_2RR at cathode:

$$CO_2 + 2e^- + H_2O \rightarrow HCOO^- + OH^- \quad (1)$$

$$2H_2O + 2e^- \rightarrow H_2 + 2OH^- \quad (2)$$

$$CO_2 + OH^- \rightarrow HCO_3^- \quad (3)$$

$$HCO_3^- + OH^- \rightarrow CO_3^{2-} + H_2O \quad (4)$$

To further explore the difference between the AEM and CEM, the onset potentials of the Cu/Sn electrode by using the AEM and CEM were -0.57 V_{RHE} and -0.62 V_{RHE}, respectively (the inset in Figure 3(A)). Additionally, the cell voltage of the AEM (3.17 V) was lower than that of the CEM (3.7 V) in Figure S8. The analysis of EIS in Figure 3 (B) showed a lower CTR (0.996 Ω) of the AEM than that of the CEM (1.136 Ω). Overall, the AEM exhibited better CO_2RR performance than the CEM in the kinetic reaction due to the smaller resistance and lower cell voltage in our home-made flow MEA reactor.

4 Conclusions

In this work, a high-performance continuous flow MEA reactor based a self-growing Cu/Sn bimetallic electrocatalysts in the liquid-phase is prepared to production of formate. This flow MEA reactor shows excellent formate selectivity (89.56%), great current density (47.56 mA·cm^{-2} at -0.91 V_{RHE}) and durable stability (20 h), which is superior to the H-type reactor owing to the higher solubility of CO_2, shorter distance between the electrodes, lower ohmic resistance and charge transfer resistance. Furthermore, the AEM has better CO_2RR performance than CEM in the kinetic reaction due to the smaller resistance (0.996 Ω) and lower cell voltage (3.17 V) in our home-made flow MEA reactor.

Acknowledgements:

The authors thank the "Scientific and Technical Innovation Action Plan" Basic Research Field of Shanghai Science and Technology Committee (19JC1410500), the financial support from the National Natural Science Foundation of China (91645110), the Fundamental Research Funds for the Central Universities (2232018A3-06).

References:

[1] Daiyan R, Saputera W H, Masood H, Leverett J, Lu X Y, Amal R. A disquisition on the active sites of heterogeneous catalysts for electrochemical reduction of CO_2 to value-added chemicals and fuel[J]. Adv. Energy Mater., 2020, 11(10): 1903796.

[2] Song R B, Zhu W, Fu J, Chen Y, Liu L, Zhang J R, Lin Y, Zhu J J. Electrode materials engineering in electrocatalytic CO_2 reduction: energy input and conversion efficiency[J]. Adv. Mater., 2020, 27(32): 1902106.

[3] Yao Y, Wang J, Shahid U B, Gu M, Wang H J, Li H, Shao M H. Electrochemical synthesis of ammonia from nitrogen under mild conditions: current status and challenges, electrochem[J]. Energy Rev., 2020, 3(2): 239-270.

[4] Al-Mamoori A, Krishnamurthy A, Rownaghi A A, Rezaei F. Carbon capture and utilization update[J]. Energy Technology, 2017, 5(6): 834-849.

[5] Kondratenko E V, Baltrusaitis G, Mul J, Larrazabal G O, Perez-Ramirez J. Status and perspectives of CO_2 conversion into fuels and chemicals by catalytic, photocatalytic and electrocatalytic processes[J]. Energy & Environ. Sci., 2013, 6(11): 3112-3135.

[6] Jhong H R, Ma S C, Kenis P J A. Electrochemical conversion of CO_2 to useful chemicals: current status, remaining challenges, and future opportunities[J]. Curr. Opin. Chem. Eng., 2013, 2(2): 191-199.

[7] Lu Q, Jiao F. Electrochemical CO_2 reduction: Electrocatalyst, reaction mechanism, and process engineering[J]. Nano Energy, 2016, 29(SI): 439-456.

[8] Zheng X, Cai Z P, Li Y S. Data linkage in smart internet of things systems: A consideration from a privacy perspective[J]. IEEE Commun. Mag., 2018, 56(9): 55-61.

[9] Liu L X, Zhou Y, Chang Y C, Zhang J R, Jiang L P, Zhu W, Lin Y. Tuning Sn_3O_4 for CO_2 reduction to formate with ultra-high current density[J]. Nano Energy, 2020, 77: 105296.

[10] Li Q Q, Rao X F, Sheng J W, Xu J, Yi J, Liu Y Y, Zhang J J. Energy storage through CO_2 electroreduction: A brief review of advanced Sn-based electrocatalysts and electrodes[J]. J. CO_2 Util., 2018, 27: 48-59.

[11] Jiang X X, Wang X K, Liu Z J, Wang Q L, Xiao X, Pan H P, Li M, Wang J W, Shao Y, Peng Z Q, Shen Y, Wang M K. A highly selective tin-copper bimetallic electrocatalyst for the electrochemical reduction of aqueous CO_2 to formate[J]. Appl. Catal. B: Environ., 2019, 259: 118040.

[12] Xiong W, Yang J, Shuai L, Hou Y, Qiu M, Li X Y, Leung M K H. CuSn alloy nanoparticles on nitrogen-doped graphene for electrocatalytic CO_2 reduction[J]. ChemElectroChem, 2019, 6(24): 5951-5957.

[13] Chen A, Lin B L. A simple framework for quantifying electrochemical CO_2 fixation[J]. Joule, 2018, 2(4): 594-606.

[14] Lee J, Lim J, Roh C W, Whang H S, Lee H. Electrochemical CO_2 reduction using alkaline membrane electrode assembly on various metal electrodes[J]. J. CO_2 Util., 2019, 31: 244-250.

[15] Ju W, Jiang F, Ma H, Pan Z, Zhao Y B, Pagani F, Rentsch

D, Wang J, Battaglia C. Electrocatalytic reduction of gaseous CO_2 to CO on Sn/Cu-nanofiber-based gas diffusion electrodes[J]. Adv. Energy Mater., 2019, 9(32): 1901514.

[16] Kim H Y, Choi I, Ahn S H, Hwang S J, Yoo S J, Han J, Kim J, Park H, Jang J H, Kim S K. Analysis on the effect of operating conditions on electrochemical conversion of carbon dioxide to formic acid[J]. Int. J. Hydrogen Energy, 2014, 39(29): 16506-16512.

[17] Gabardo C M, O'Brien C P, Edwards J P, McCallum C, Dinh Y, Xu C T, Sargent J, Li E H, Sinton D. Continuous carbon dioxide electroreduction to concentrated multi-carbon products using a membrane electrode assembly [J]. Joule, 2019, 3(11): 2777-2791.

[18] Zhang F, Jin Z, Chen C, Tang Y, Mahyoub S A, Yan S, Cheng Z. Electrochemical conversion of CO_2 to CO into a microchannel reactor system in the case of aqueous electrolyte[J]. Ind. Eng. Chem. Res., 2020, 59(13): 5664-5674.

[19] Yang H Z, Kaczur J J, Sajjad S D, Masel R I. Electrochemical conversion of CO_2 to formic acid utilizing sustainion (TM) membranes[J]. J. CO_2 Util., 2017, 20: 208-217.

[20] Larrazabal G O, Strom-Hansen P, Heli J P, Zeiter K, Therkildsen K T, Chorkendorff I, Seger B. Analysis of mass flows and membrane cross-over in CO_2 reduction at high current densities in an MEA-type electrolyzer[J]. ACS Appl. Mater. Inter., 2019, 11(44): 41281-41288.

[21] Liu J Y, Peng L W, Zhou Y, Lv L, Fu J, Lin J, Guay D, Qiao J L. Metal-organic-frameworks-derived Cu/Cu_2O catalyst with ultrahigh current density for continuous-flow CO_2 electroreduction[J]. ACS Sustain. Chem. Eng., 2019, 7(18): 15739-15746.

[22] Gong Q F, Ding P, Xu M Q, Zhu X R, Wang M Y, Deng J, Ma Q, Han N, Zhu Y, Lu J, Feng Z X, Li Y F, Zhou W, Li Y G. Structural defects on converted bismuth oxide nanotubes enable highly active electrocatalysis of carbon dioxide reduction[J]. Nat. Commun., 2019, 10(1): 2807.

[23] Cifrain M, Kordesch K V. Advances, aging mechanism and lifetime in AFCs with circulating electrolytes[J]. J. Power Sources, 2004, 127: 234-242.

[24] Peng L W, Wang Y X, Masood I, Zhou B, Wang Y F, Lin J, Qiao J L, Zhang F Y. Self-growing Cu/Sn bimetallic electrocatalysts on nitrogen-doped porous carbon cloth with 3D-hierarchical honeycomb structure for highly active carbon dioxide reduction[J]. Appl. Catal. B-Environ., 2020, 264: 118447.

[25] Xiang H, Miller H A, Bellini M, Christensen H, Scott K, Rasul S, Yu E H. Production of formate by CO_2 electrochemical reduction and its application in energy storage [J]. Sustain. Energ. Fuels, 2020, 4(1): 277-284.

[26] Hatsukade T, Kuhl K P, Cave E R, Abram D N, Jaramillo T F. Insights into the electrocatalytic reduction of CO_2 on metallic silver surfaces[J]. Phys. Chem. Chem. Phys., 2014, 16(27): 138-149.

[27] Burdyny T, Smith W A. CO_2 reduction on gas-diffusion electrodes and why catalytic performance must be assessed at commercially-relevant conditions[J]. Energ. Environ. Sci., 2019, 12(5): 1442-1453.

一种用于电还原 CO_2 生成甲酸的高性能连续流动式 MEA 反应器

刘佩璇[1#],彭芦苇[1#],何瑞楠[1],李露露[1],乔锦丽[1,2*]

(1. 东华大学环境科学与工程学院,上海 201620; 2. 上海市污染控制与生态安全研究所,上海 200092)

摘要: 电化学二氧化碳还原反应(CO_2RR)是一种利用间歇性可再生电力缓解环境问题,并且生产液体燃料和工业化学品的有前途的方法。然而,传统的 H 型反应器由于在电解液中较低的 CO_2 溶解度以及两电极之间较大的极距而导致高欧姆电阻,严重限制了 CO_2RR 的电化学性能,不利于 CO_2RR 在工业应用的发展。在本文中,我们设计了一种基于 0.5 mol·L^{-1} $KHCO_3$ 的自生长 Cu/Sn 双金属电催化剂的高性能连续流膜电极组件(MEA)反应器,用于将 CO_2 转化为甲酸。与 H 型反应器相比,流动式 MEA 反应器不仅显示出优异的电流密度(-1.11 V_{RHE} 时电流密度为 66.41 mA·cm^{-2}),而且还保持了较高的甲酸法拉第效率(89.56%),并且能够稳定工作至少 20 h。本文还设计了一套新型 CO_2RR 系统,可以有效地分离气态/液态产物。出乎意料的是,在 -0.91 V_{RHE} 且电池电压为 3.17 V 时,甲酸的生产率为 163 μmol·h^{-1}·cm^{-2}。本文为克服电化学 CO_2RR 的传质限制以及分离液体和气体产物提供了一条新途径。

关键词: 电化学还原;二氧化碳;流动式 MEA 反应器;电解槽